Supplement of The Cryosphere, 16, 2421–2448, 2022
https://doi.org/10.5194/tc-16-2421-2022-supplement

The Cryosphere Open Access EGU

Supplement of

Controls on Greenland moulin geometry and evolution from the Moulin Shape model

Lauren C. Andrews et al.

Correspondence to: Lauren C. Andrews (lauren.c.andrews@nasa.gov)

Elastic deformation around a cylindrical hole in ice

Supplement **S1** for "Controls on Greenland moulin geometry and evolution from the Moulin Shape model", *The Cryosphere*.

Contents

S1.1 Introduction

Here we describe the derivation of the elastic deformation component of the MouSh model. It is based on Aadnøy (1987).

Bernt Aadnøy, a petroleum engineer, derived expressions for the stresses surrounding a borehole (wellbore) through competent rock (Aadnøy, 1987). He applied the Kirsch (1898) solutions for a circular hole in a plate, stacking many plates to achieve a borehole. He derives an ana-lytic solution for the stress field near a cylindrical borehole through a uniform, solid (non-porous) medium. From the stress solution, we derive the resulting strains using an elastic constitutive relation (Hooke's Law) and integrate the strains to get the total elastic deformation at the borehole wall. We take this borehole through rock as a direct analogue to a moulin through ice.

We treat the moulin as a stack of independent plates, each with a hole in them, of radius a. The radius of the hole in each plate (equivalently, at each elevation z) is independent of the radius in the plate above and below, but generally, $a(z)$ is smoothly varying because the forces at each z are smoothly varying.

S1.2 Aadnøy's setup and stress solutions

Aadnøy (1987) finds the stress field around a borehole by summing the independent stress contributions from three sources: hydrostatic stress ($P = P_w - P_i = \rho_w g(h_w - z) - \rho_i g(H_i - z)$), deviatoric stresses ($\sigma_x$ and σ_y), and shear stress (τ_{xy}). The sign of the pressure P is "positive outward", i.e., net water pressure ($P_w > P_i$) opens the moulin and net ice pressure ($P_i > P_w$) closes the moulin.

S1.2.1 Assumptions

The Aadnøy (1987) solution is based on the Kirsch (1898) equations, which describe the stresses around a hole when the rock is subject to deviatoric stress in one direction, but elaborates from them by adding a second deviatoric stress, a shear stress, and pressure. The Kirsch (1898) and Aadnøy (1987) equations assume that the rock (ice) is a competent linear elastic material. The Kirsch (1898) solution is appropriate for a material stressed below its elastic limit, or roughly one half its compressive strength (Goodman, 1989). The compressive strength of ice is 3–10 MPa (Fransson, 2009), making the elastic limit 1–5 MPa. This is equivalent to the cryostatic pressure in an empty borehole in ice 100–500 m thick, or the cryo/hydrostatic pressure in a borehole in ice 1–6 km thick that is water-filled to flotation. Because moulin water levels are typically $>\sim 50\%$ the flotation level and ice thicknesses are of order $\sim$100–1000 m, moulins meet these requirements. We note that toward the beginning or end of the melt season (when water levels are lowest), and in thick ice ($>\sim$1000 m), the ice surrounding the moulin likely approaches or may exceed the elastic limit.

Aadnøy (1987) assumes plane strain in z, i.e., ϵ_z=0 (no vertical deformation anywhere). This is consistent with the assumptions of our overall MouSh model and is the most basic formulation in solid mechanics. The total absence of vertical deformation in the face of finite horizontal deformation can be accommodated by an effective infinite domain in the cross-sectional plane of the moulin (xy). We happen to make this assumption anyway by summing elastic deformation from the point at infinity to the moulin wall (Sect. S1.3).

Alternately, Aadnøy (1987) also presents a plane stress solution. Plane strain is appropriate for thin plates with free surfaces (the top and bottom, z-facing surfaces), which differs from our "stack of plates" domain because our stacked plates have no free surfaces (excepting the topmost and bottommost plates). Aadnøy (1987)'s plane stress solution differs by a factor of $\frac{1+\nu}{1+\nu+\nu^2}$ from the plane strain solution (Goodman, 1989); for $\nu = 0.3$, this is a change of 7%. The difference is small and plane stress is a less appropriate formulation than plane strain.

S1.2.2 Solution

The Aadnøy (1987) solution is in cylindrical coordinates (r, θ, z). The radius of the hole is a. Figure S1 shows the problem geometry.

The Kirsch (1898) equations for stresses around a hole in an infinite plate made of an elastic material are as follows:

$$\sigma_r = \frac{\Delta\sigma_x + \Delta\sigma_y}{2}\left(1 - \frac{a^2}{r^2}\right) + \frac{\Delta\sigma_x - \Delta\sigma_y}{2}\left(1 + \frac{3a^4}{r^4} - \frac{4a^2}{r^2}\right)\cos 2\theta + \Delta\tau_{xy}\left(1 + \frac{3a^4}{r^4} - \frac{4a^2}{r^2}\right)\sin 2\theta + \frac{a^2}{r^2}\Delta P$$
$$\sigma_\theta = \frac{\Delta\sigma_x + \Delta\sigma_y}{2}\left(1 + \frac{a^2}{r^2}\right) - \frac{\Delta\sigma_x - \Delta\sigma_y}{2}\left(1 + \frac{3a^4}{r^4}\right)\cos 2\theta - \Delta\tau_{xy}\left(1 + \frac{3a^4}{r^4}\right)\sin 2\theta - \frac{a^2}{r^2}\Delta P$$
$$\sigma_z = \Delta\sigma_{zz} - 2\nu\left(\Delta\sigma_x - \Delta\sigma_y\right)\frac{a^2}{r^2}\cos 2\theta - 4\nu\Delta\tau_{xy}\frac{a^2}{r^2}\sin 2\theta \tag{S1}$$

Here, ΔP is the change in pressure around the borehole. In the rock mechanics example, ΔP is equivalent to P, the pressure, because it assumes the borehole was recently drilled. For the moulin case, where the water level fluctuates by the minute, ΔP is the change in pressure over the time interval in question. The same applies to the deviatoric stresses $\Delta\sigma_x$ and $\Delta\sigma_y$ and the shear stress $\Delta\tau_{xy}$: these are changes in the stress field over a time interval.

Applying Hooke's Law to these equations yields the corresponding strain at any point in the domain. Hooke's Law is just a linear combination of the three stresses in Eq. (S1):

$$\epsilon_r = E^{-1}\left(\sigma_r - \nu\left(\sigma_\theta + \sigma_z\right)\right)$$
$$\epsilon_\theta = E^{-1}\left(\sigma_\theta - \nu\left(\sigma_r + \sigma_z\right)\right) \tag{S2}$$
$$\epsilon_z = E^{-1}\left(\sigma_z - \nu\left(\sigma_r + \sigma_\theta\right)\right)$$

where E is Young's modulus ($\sim$1 GPa) and ν is Poisson's ratio ($\sim$0.3 for ice; unitless).

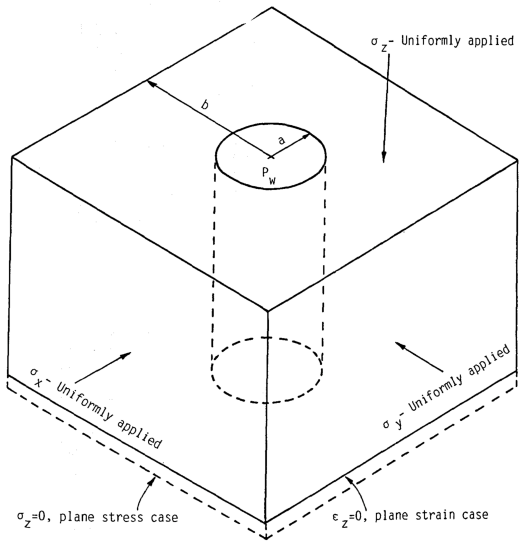

Figure S1. *Problem setup, adapted from Aadnøy (1987), of a borehole in a rock medium. We adapt this to a cylindrical moulin through ice. We use the plane strain case, although the plane stress case is equivalent within 7%.*

S1.3 Integrated elastic deformation

To calculate the radial expansion or contraction of moulin size, we must know the total elastic deformation of the moulin wall. This is the spatial integral of ϵ_r, from the borehole wall ($r = a$) to the end of the domain ($r = \infty$). Deformation will be greatest at the borehole wall ($r = a$) and will fall off to zero as $r \to \infty$.

Integrating Eq. (S2) over $r|_{\infty}^{a}$ entails integrating each stress from Eq. (S1) over the same limits, then summing them together with the appropriate constants involved. So, must simply integrate all the *r-dependent* terms in the Eq. (S1) stresses over $r|_{\infty}^{a}$. We ignore any constant (r-independent) terms in Eq. (S1) because these do not contribute to spatially varying deformation.

Eq. (S1) with the constants removed are as follows:

$$\begin{aligned}
\sigma_r^* = &\quad \left(\Delta P - \frac{\Delta\sigma_x + \Delta\sigma_y}{2}\right)\left(\frac{a^2}{r^2}\right) + \left(\frac{\Delta\sigma_x - \Delta\sigma_y}{2}\cos 2\theta + \Delta\tau_{xy}\sin 2\theta\right)\left(\frac{3a^4}{r^4} - \frac{4a^2}{r^2}\right) \\
\sigma_\theta^* = &- \left(\Delta P - \frac{\Delta\sigma_x + \Delta\sigma_y}{2}\right)\left(\frac{a^2}{r^2}\right) - \left(\frac{\Delta\sigma_x - \Delta\sigma_y}{2}\cos 2\theta + \Delta\tau_{xy}\sin 2\theta\right)\left(\frac{3a^4}{r^4}\right) \\
\sigma_z^* = &\left(-2\nu\left(\Delta\sigma_x - \Delta\sigma_y\right)\cos 2\theta - 4\nu\Delta\tau_{xy}\sin 2\theta\right)\left(\frac{a^2}{r^2}\right)
\end{aligned} \tag{S3}$$

Indefinite integrals of Eq. (S3) are as follows:

$$\begin{aligned}
\int \sigma_r^* dr &= \left(2\Delta P - \left(\Delta\sigma_x + \Delta\sigma_y\right)\right)\left(\frac{a^2}{2r}\right) + \left(\left(\Delta\sigma_x - \Delta\sigma_y\right)\cos 2\theta + 2\Delta\tau_{xy}\sin 2\theta\right)\left(\frac{2a^2}{r} - \frac{3a^4}{2r^3}\right) \\
\int \sigma_\theta^* dr &= -\left(2\Delta P - \left(\Delta\sigma_x + \Delta\sigma_y\right)\right)\left(\frac{a^2}{2r}\right) + \left(\left(\Delta\sigma_x - \Delta\sigma_y\right)\cos 2\theta + 2\Delta\tau_{xy}\sin 2\theta\right)\left(\frac{3a^4}{2r^3}\right) \\
\int \sigma_z^* dr &= 2\nu\left(\frac{a^2}{r}\right)\left(\left(\Delta\sigma_x - \Delta\sigma_y\right)\cos 2\theta + 2\Delta\tau_{xy}\sin 2\theta\right)
\end{aligned} \tag{S4}$$

These all have dimensions of `Pa·m`.

Next, we evaluate definite integrals of Eq. (S4), over $r|_{\infty}^{a}$. Every term in the $r \to \infty$ expressions go to zero. Similarly, all tangential variations (coordinate θ) do not affect moulin size, so we replace all $\cos 2\theta$ or $\sin 2\theta$ with its average absolute value, $\frac{1}{2}$. This gives

$$\begin{aligned}
\int_{\infty}^{r} \sigma_r^* dr &= a\left(\quad \Delta P - \frac{1}{2}(\Delta\sigma_x + \Delta\sigma_y) + \frac{1}{4}(\Delta\sigma_x - \Delta\sigma_y) + \frac{1}{2}\tau_{xy}\right) \\
\int_{\infty}^{r} \sigma_\theta^* dr &= a\left(-\Delta P + \frac{1}{2}(\Delta\sigma_x + \Delta\sigma_y) + \frac{3}{4}(\Delta\sigma_x - \Delta\sigma_y) + \frac{3}{4}\Delta\tau_{xy}\right) \\
\int_{\infty}^{r} \sigma_z^* dr &= \nu a\left(\left(\Delta\sigma_x - \Delta\sigma_y\right) + 2\Delta\tau_{xy}\right)
\end{aligned} \tag{S5}$$

Finally, we take a linear combination of Eqs. (S5): a sum with the appropriate coefficients from Hooke's Law (Eq. S2) to get the strain in the r, θ, and z directions, although we discard strain in the θ or z directions. We thus obtain u_r, the total radial deformation in r, by $u_r = \int_{\infty}^{a} \epsilon_r dr$.

$$u_r = \int_{\infty}^{a} \epsilon_r dr = E^{-1}\left[\int_{\infty}^{a} \sigma_r^* dr - \nu\left(\int_{\infty}^{a} \sigma_\theta dr + \int_{\infty}^{a} \sigma_z dr\right)\right]$$
$$= \frac{a}{E}\left[(1+\nu)\left(\Delta P - \frac{1}{2}(\Delta\sigma_x + \Delta\sigma_y)\right) + \frac{1}{4}(\Delta\sigma_x - \Delta\sigma_y)(1 - 3\nu - 4\nu^2) + \frac{1}{4}\Delta\tau_{xy}(2 - 3\nu - 8\nu^2)\right]$$
$$\text{for } \Delta P = \rho_w g(\Delta h_w - z) - \rho_i g(\Delta H_i - z) = \Delta P_w - \Delta P_i \tag{S6}$$

In the moulin model, we assume that all pressure changes ΔP are due to changes in water level Δh_w and that the ice thickness H_i stays constant. Thus, $\Delta P = \rho_w g(\Delta h_w - z) = \Delta P_w$.

As a check, the integrated displacement u_r (Eq. S6) increases with moulin radius a. This makes sense as a tighter radius of curvature (low a) is more difficult to deform radially (low u_r). Inward deformation (moulin closure) will have negative u_r and outward deformation (moulin expansion) will have positive u_r.

For a typical Greenland Ice Sheet moulin with radius a ~1 meter, the pressure change associated with Δh_w ~1 meter will induce elastic deformation of a few micrometers. This water level change would typically occur over many minutes to a few hours, yielding elastic deformation of up to some 10^{-4} meters per day.

S1.4 Simplest case: Non-varying deviatoric and shear stresses

The deviatoric and shear stresses σ_x, σ_y and τ_{xy} are generally not well know and are variable from place to place in the ablation zone. The spatial variation typically occurs over scales of a few kilometers, and the range may be roughly [–50 kPa +50 kPa]. However, Eq. (S6) uses their changes over a time interval, $\Delta\sigma_x$, $\Delta\sigma_y$ and $\Delta\tau_{xy}$. For a moulin advecting through the ablation zone at ~100 m/yr, the stress changes $\Delta\sigma_x$, $\Delta\sigma_y$ and $\Delta\tau_{xy}$ are trivial (~1 kPa) over a melt season. Thus, we make a further simplification that $\Delta\sigma_x = \Delta\sigma_y = \Delta\tau_{xy} = 0$, which yields the most basic expression for radial elastic deformation u_r:

$$u_r = \frac{a}{E}(1+\nu)\Delta P \tag{S7}$$

This is the same equation as is commonly used for dilatometer testing in rock mechanics (Goodman, 1989, page 190).

S1.5 Instantaneous elastic deformation and calculated deformation rates

Elastic displacement is an instantaneous process that occurs in reaction to a change in stress. In the case of a moulin during the melt season, the water level in the moulin changes essentially

continuously, which induces continuous changes in pressure (ΔP), which drives continuous elastic deformation (Eqs. S6 and S7), although we calculate it only once per timestep. To compare elastic deformation (instantaneous) to viscous deformation (occurring over a time interval), we assume the deformation rate occurs over the entire timestep:

$$\text{elastic deformation rate} = \frac{u_r}{\Delta t} \tag{S8}$$

This is analogous to how we calculate a viscous deformation rate or a rate of refreezing.

More precisely, one could express this in terms of the rate of pressure change, $\frac{\Delta P}{\Delta t}$:

$$\frac{u_r}{\Delta t} = \frac{a}{E}(1+\nu)a\frac{\Delta P}{\Delta t} \tag{S9}$$

This approach assumes that the water pressure varies smoothly over the time interval in question. This is generally true: we run the model at 5-minute timesteps, and the most common discontinuous variations in pressure are likely sourced from rain storms or other sudden melt events (time scales of hours).

References

Aadnøy, B. S.: A complete elastic model for fluid-induced and insitu generated stresses with the presence of a borehole, EnergySources, 9, 239–259, 1987.

Fransson, L.: Ice Handbook for Engineers, Version 1.2, Lulea Tekniska Universitet, 1-31, 2009.

Goodman, R. E.: Introduction to Rock Mechanics, 2nd ed., Wiley, New York, ISBN 0-471-81200-5, 1989.

Kirsch, G. E.: Die Theorie der Elastizität und die Bedürfnisse der Festigkeitslehre. Zeitschrift des Vereines deutscher Ingenieure, 42, 797–807, 1898.

MouSh sensitivity to model choices

Supplement **S2** for "Controls on Greenland moulin geometry and evolution from the Moulin Shape model", *The Cryosphere.*

S2.1 The impact of diurnal supraglacial variability

Under steadily varying conditions, the modeled moulin should reach a quasi-equilibrium state independent of initial conditions with melting opposing viscous and elastic deformation below the water line and the only change being driven by shear deformation. We examine the quasi-equilibrium state and the impact of supraglacial variability on this state. Increasing the amplitude of the diurnal Q_{in} signal results in an increase in the mean water level but very little change in the moulin radius at the mean water level apart from an amplitude of zero (Fig. S2). The magnitude of the Q_{in} signal impacts both the mean moulin water level and the radius at that water level (Fig. S3). The changes in mean moulin water level in response to variations in Q_{in} amplitude and magnitude are non-linear (Fig. S4). Further description is included in Sect. 2.5.1 and 3.1.

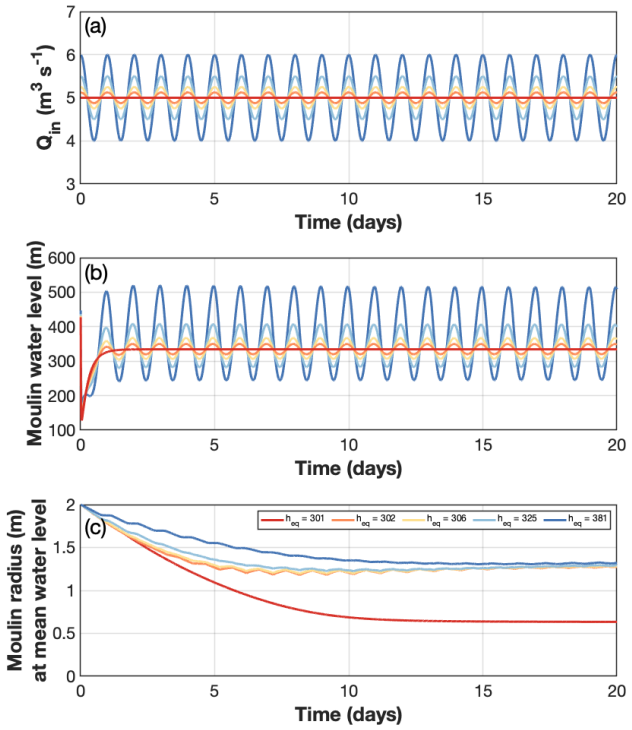

Figure S2. The impact of the Q_{in} amplitude (a) on moulin water level (b) and the major moulin radius at the mean moulin water level over the last 24 h (c) for five different Q_{in} amplitudes, 0 m^3 s^{-1} (red), 0.25 m^3 s^{-1} (orange), 0.5 m^3 s^{-1} (dark yellow), 1 m^3 s^{-1} (mid-blue), 2 m^3 s^{-1} (dark blue). Mean or quasi-equilibrium water levels indicated in (c). All runs have a magnitude of 5 m^3 s^{-1}. Ice thickness is 553 m with flotation at approximately 503 m.

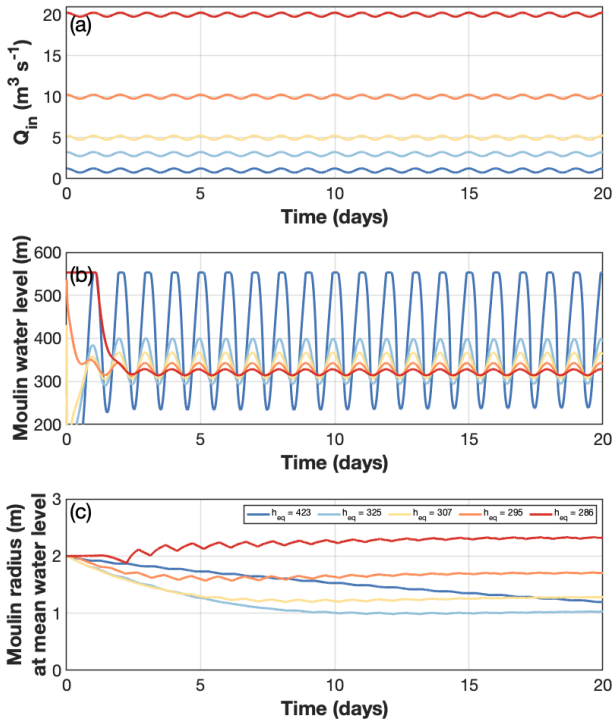

Figure S3. The impact of the Q_{in} magnitude (a) on moulin water level (b) and the major moulin radius at the mean moulin water level over the last 24 h (c) for five different Q_{in} magnitudes, 1 m^3 s^{-1} (blue) 3 m^3 s^{-1} (light blue), 5 m^3 s^{-1} (dark yellow), 10 m^3 s^{-1} (orange), 20 m^3 s^{-1} (red). Mean water levels indicated in (c). All runs have an amplitude of 0.5 m^3 s^{-1}. Ice thickness is 553 m with flotation at approximately 503 m.

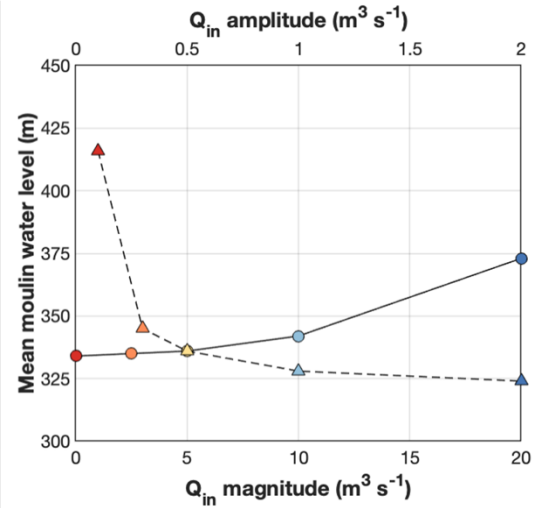

Figure S4. Mean moulin water level as a function of Q_{in} magnitude (triangles) and amplitude (circles). Colored as indicated in Figures S6 and S7: Q_{in} magnitudes, 1 m^3 s^{-1} (red), 3 m^3 s^{-1} (orange), 5 m^3 s^{-1} (dark yellow), 10 m^3 s^{-1} (light blue), 20 m^3 s^{-1} (blue); Q_{in} amplitudes, 0 m^3 s^{-1} (red), 0.25 m^3 s^{-1} (orange), 0.5 m^3 s^{-1} (dark yellow), 1 m^3 s^{-1} (light blue), 2 m^3 s^{-1} (dark blue).

S2.2 Sensitivity to model choices

We perform a set of experiments to examine the impact of various parameterizations and model choices on the MouSh modeled moulin water level and moulin capacity, two components of a moulin that can directly impact the englacial and subglacial hydrologic systems. In each model run, all characteristics and forcings are kept the same as in the control run, except the parameterization or value of interest. Specific details are detailed below, and the results of these exploratory runs are in Figure S5 and Figure S6. All moulin water level differences are presented as *test – control* and percentage differences are *(test – control) / control*.

S2.2.1 Control run

The control run is the Basin 1 experiment detailed in Sect. 2.5.2 and Table 2, with the exception that diurnal variability of Q_{in} is reduced by 30% to prohibit prolonged periods when daily peak water levels overtop the moulin.

S2.2.2 Circular geometry (Experiment 1)

The circular run prescribes a circular instead of a semi-elliptical cross-sectional area. In practice, this simply means that open channel melting above the water line is applied uniformly around the moulin perimeter (instead of only to r_2 as in the semi-elliptical formulation) such that the moulin plan view cross-sectional area is circular and only one radius is evolved. Deformation due to elastic, viscous and turbulent melting below the water line is then only calculated for the single radius. This parameterization removes any asymmetry. Both runs have the same initial circular plan view cross-sectional area.

The use of a circular geometry has little impact on moulin water level over the course of the melt season (Fig. S5a). Compared to the control run, the circular geometry generally exhibits slight increases in moulin water level (< 0.5 m). These increases become slightly higher at higher Q_{in} values. The primary difference comes in the moulin capacity: the circular geometry can to 31% smaller than the control moulin as the end of the melt season approaches (Fig. S5b). This difference is concentrated in regions that are not generally water filled except at high water levels, thus has limited impact on moulin water level. This difference is the result of the control moulin run becoming more elliptical.

S2.2.3 Elastic deformation (Experiment 2)

For completeness, we include elastic deformation within the moulin model. Our formulation is dependent on the change in moulin water level and moulin radii (Supplement Sect. 1). Thus, elastic deformation within MouSh is substantially smaller than viscous deformation due to the relatively small moulin radii modeled here. We examine whether the inclusion of elastic deformation impacts moulin water level and capacity by performing a run without elastic deformation.

In its current formulation, the exclusion of elastic deformation has almost no impact on moulin water level and capacity (Fig. S5c and d). This comparison suggests that the simplifying case (*no elastic deformation*) has minimal impact on the model results.

S2.2.4 Distance from terminus (Experiment 3)

In our parameterization of the subglacial model, the hydraulic gradient is set by the water level in the moulin and the distance from the terminus. Because the hydraulic gradient exerts an important control over both the subglacial channel and moulin evolution, we examine the impact of different subglacial lengths (L). We compare the control run, L = 13.6 km, to model runs with one half, L = 6.8 km, and one and one half, L =20.4 km, while using the same ice thickness (553 m). This change directly impacts the hydraulic gradient calculated in Eq. (24).

Modifying the distance from terminus and the associated hydraulic gradient can result in substantial changes to both the moulin water level (+/– ~100m) and moulin capacity (+/– ~30%; Fig. S5e and f). Shortening L reduces both moulin water level and moulin capacity. Lower water levels reduce water velocities and allows viscous and elastic deformation to increase, resulting in a smaller moulin. While increasing L results in higher moulin water levels and a larger moulin. Higher moulin water levels increase turbulent melting linearly and reduce viscous and elastic deformation non-linearly. In addition, with a longer L, the moulin has more instances of water level being above floatation, which permits viscous and elastic deformation to open the moulin. The difference in moulin water levels

tends to be exacerbated during higher Q_{in} values (Fig. S5e), resulting in larger differences from the control run during the middle of the melt season and less impact during the onset and cessation of melting.

S2.2.5 Base flow (Experiment 4)

Our simple parameterization of the subglacial system means that the model represents only a single moulin and a long channel. This is an oversimplification of what is generally a complex arborescent network (e.g., Werder et al., 2013) with multiple moulins along a single channel (Andrews et al., 2014). To parameterize this connectivity, we prescribe a base flow term to be five times the 5-day lagged moving average moulin input directly into the subglacial channel (Fig. 6a). This definition removes diurnal signals but preserves melt events and the seasonal pattern of melt. Without baseflow, MouSh can produce unrealistically high-water levels with realistic meltwater inputs. While an alternative would be to either substantially dampen the diurnal variability or increase moulin inputs, we believe that our current approach best approximates the natural system. Unfortunately, prescribing a larger initial subglacial cross-sectional area does not mitigate the above problem because moulin and subglacial channel size are not dependent on the initial conditions after the first few weeks. Here we examine the impact of reducing the base flow to two times the 5-day lagged moving average.

The prescribed base flow acts to maintain a larger subglacial channel and permits more rapid growth due to melting; this behavior is non-linear. Therefore, reducing the amount of base flow into the subglacial system reduces the ability of the subglacial channel to accommodate the large diurnal swings in Q_{in}. Therefore, a reduction in base flow results in higher moulin water levels for much of the model run (Fig. S5g). Interestingly, during diurnal minimums, the water levels are lower in the low base flow run relative to the control (negative values in Fig S5g). This is likely due to greater moulin growth (increased turbulent melting and reduced or negative viscous and elastic deformation) associated with higher water levels. The moulin capacity difference displays a clear seasonal pattern (Fig. S5h). During the tails of the melt season, the lower base flow run exhibits a similar capacity to the control, but as diurnal variability and maximum daily water levels increase, the low baseflow moulin begins to grow relative to the control moulin.

S2.2.6 Static subglacial geometry (Experiment 5)

The MouSh model is meant to model moulin geometry. However, to permit water flow through the moulin, we include a simple time-evolving subglacial channel (Sect. 2.4.2). A fixed subglacial channel would, in essence, provide the simplest subglacial component. However, a fixed subglacial channel results in both extremely low and extremely high moulin water levels when Q_{in} values are both high and low, respectively; therefore, during an experiment with seasonally evolving Q_{in}, the subglacial channel size must be chosen very carefully to produce vaguely realistic moulin water levels and capacities. Therefore, we examine the impact of fixing the subglacial cross-sectional area S using a co-sinusoidal supraglacial of 40 days,as described in Eq. (22). For this comparison, we fix $S = 1.95$ m^2 (*Fixed S*), which is equal to the mean value of the subglacial channel cross-sectional area in the control experiment; this minimizes differences between the runs.

The moulin with a fixed subglacial cross-sectional area has similar quasi-equilibrium water levels but less diurnal variability (Fig. 6b). The model run with a fixed subglacial channel also displays a slightly lower radius at the mean water level of the last 10 experiment days. The primary conclusion here is that the moulin geometry and variability is, at least in part, driven by the characteristics of the subglacial hydrologic model used. Such dependency is not uncommon in models of the glacial hydrologic system. For example, the presence of modeled channels is dependent on the prescribed location of supraglacial inputs and prescribed conductivity of the surrounding system. Therefore, the subglacial model used with the MouSh model should be carefully considered.

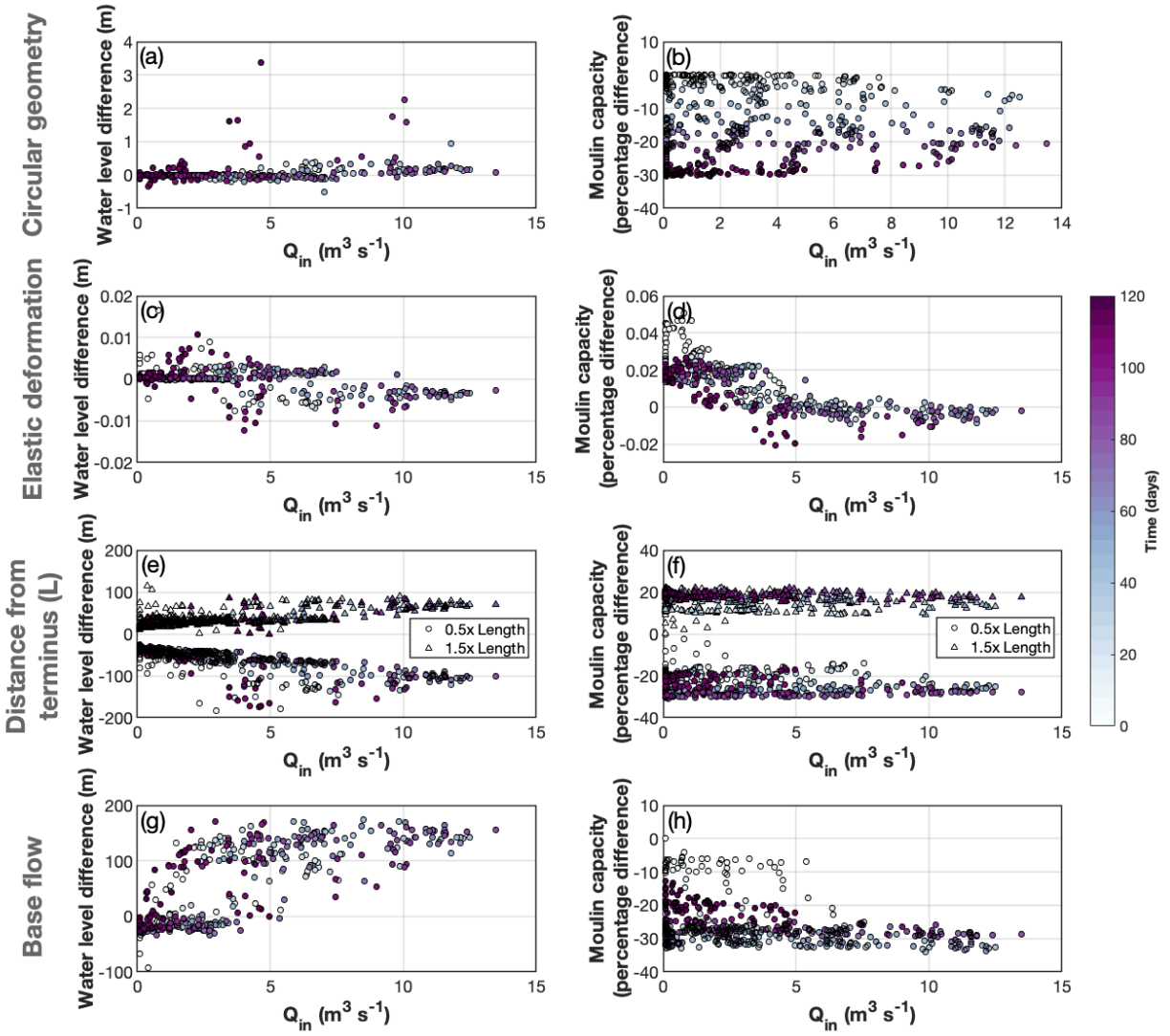

Figure S5. Moulin water level and capacity differences relative to the Basin 1 (H_i = 553 m) control run for a circular geometry (a-b); elastic deformation (c-d); varying distances from the terminus or subglacial path length (L; e-f); and a reduced baseflow (g-h). In all panels on the left-hand side, the differences are experiment minus control. In all panels on the right-hand side, moulin capacity is plotted as a percent difference from the control run such that positive values indicate a capacity larger than the control run and negative values indicate a capacity smaller than the control run.

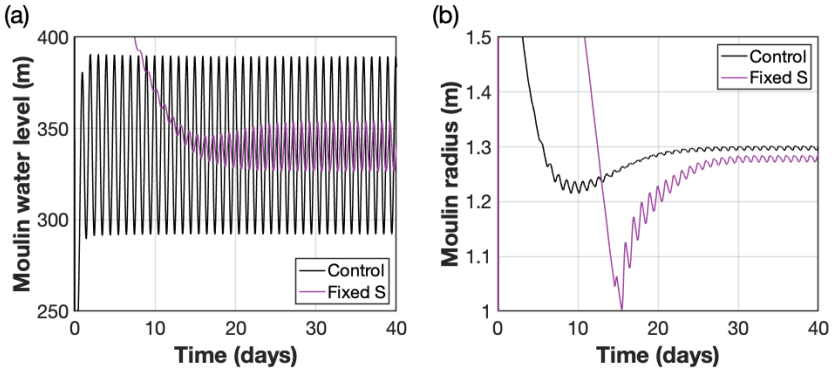

Figure S6. Moulin water level (a) and moulin radius at the mean water level (b) from experiments with variable subglacial S (*Control*; black) and a fixed subglacial cross-sectional area of 1.95 m^2 (*Fixed S*; purple).

References

Andrews, L. C., Catania, G. A., Hoffman, M. J., Gulley, J. D., Lüthi, M. P., Ryser, C., Hawley, R. L., and Neumann, T. A.: Direct observations of evolving subglacial drainage beneath the Greenland Ice Sheet, Nature, 514, 80–83, https://doi.org/10.1038/nature13796, 2014.

Werder, M. A., Hewitt, I. J., Schoof, C. G., and Flowers, G. E.: Modeling channelized and distributed subglacial drainage in two dimensions, *J. Geophys. Res. Earth Surf.*, 118,2140–2158, https://doi.org/10.1002/jgrf.20146, 2013.